FUDMA Journal of Sciences (FJS)
ISSN online: 2616-1370
ISSN print: 2645 - 2944
Vol. 10 No. 3, February, 2026, pp 306 – 313
DOI: https://doi.org/10.33003/fjs-2026-1003-4594

MODELLING AND SIMULATION OF DYNAMIC VIBRATION ANALYSIS OF ROTOR-BEARING SYSTEMS UNDER UNBALANCE AND HARMONIC EXCITATIONS

[*1]Okiemute Dickson Ofuyekpone, [2]Ochuko Goodluck Utu, [1]Oghenemaro Geraldine Eduviere, [3]Yaabari Naenwi

[1]Materials and Metallurgical Engineering Department, Southern Delta University, Ozoro, Delta State, Nigeria.
[2]Department of Welding and Fabrication Engineering, Delta State Polytechnic, Ogwashi-Uku, Delta State, Nigeria.
[3]Post Graduate Student, University of Cross River State, Calabar, Cross River State, Nigeria.

[*]Corresponding Author's Email: okedickbest@yahoo.com.

ABSTRACT

Rotor–bearing systems in rotating machinery frequently experience vibration due to mass unbalance, particularly at elevated operating speeds. While advanced multi-degree-of-freedom rotor models exist, many studies focus primarily on detailed numerical simulations without providing simplified parametric tools that assist engineers in interpreting vibration trends during preliminary design stages. This lack of transparent parametric insight represents an important gap in practical rotor dynamic analysis. This study investigates the vibration behavior of a rotor–bearing system subjected to unbalance-induced harmonic excitation using a single-degree-of-freedom (SDOF) linear dynamic model. The SDOF formulation was intentionally adopted to enable clear parametric interpretation of system behavior while preserving the essential physics of rotor vibration. To provide generalized interpretation, resonance behavior was analyzed using dimensionless parameters, including the normalized frequency ratio and damping ratio. The results demonstrate that vibration amplitude increases significantly as the normalized speed approaches unity, corresponding to the resonance region, while higher damping ratios effectively suppress vibration amplitude. Such that, at an operating speed of 388 rad/s, increasing the damping coefficient from 50 Ns/m to 100 Ns/m reduces the peak displacement from approximately 0.010 m to 0.005 m. A vital contribution of this work was the development of a speed–damping response surface, which maps peak rotor displacement as a function of operating speed and bearing damping. The proposed modeling and visualization framework offers a simple yet effective approach for preliminary rotor dynamic assessment and can support improved design and maintenance planning for rotating machinery.

Keywords: Rotor–bearing system, Unbalance excitation, Vibration analysis, Harmonic Excitation.

INTRODUCTION

Unbalance-induced vibration is one of the most common sources of dynamic instability in rotating machinery such as turbines, compressors, pumps, and electric motors. Even minor offsets between the geometric axis of the rotor and its mass center may cause centrifugal forces to increase quadratically with the rotational speed and create high lateral vibration, or may cause excessive bearing loads, shorter machine life or even catastrophic failure (Xu et al., 2025). These vibration effects become particularly critical when the operating speed approaches the system's natural frequency, resulting in resonance amplification of shaft displacement and bearing forces. (Zhang et al., 2025; Abdul et al., 2024; Su, et al, 2024). The industrial practice has standardized criteria in the assessment of vibration severity, which include ISO 10816 and ISO 20816, which classify machine condition using the level of vibration velocity or displacement at bearing housings (International Organization for Standardization, 2016 & 2022). In most industrial machines, where the power is between 15 and 300 kW, a vibration velocity of above 4.5-7.1 mm/s is deemed unacceptable and it can represent the possibility of mechanical damage or instability in the operation. The benchmarks indicate the need to know the interdependence of the operating parameters, especially the rotor speed and bearing damping related to the vibration amplitude in the rotor bearing systems (Rao, 2017; Muszynska, 2021; Wu, et al, 2023). The concept of modelling and simulation has been applied to many systems with great successes (Oke, et al., 2024; Oladele, et al., 2024)

Considerable research has been conducted on rotor dynamic modeling, starting with simplified analytical model, up to sophisticated finite element modeling with gyroscopic effects, nonlinear bearing forces, and multi-disk shaft (Rao, 2017; Friswell et al., 2010). Rotor models advanced rotor models are useful in predicting the complicated dynamic behaviour, such as mode coupling, instability, and nonlinear resonance effects (Muszynska, 2021). Recent research has applied high-fidelity numerical models to determine vibration reduction techniques in the aero engine rotor systems and flexible shaft assemblies in response to unbalance excitation (Zhang et al., 2022; Li et al., 2023). Although these models offer the detailed understanding of the system behavior, they may come with high levels of computational complexity and a great number of parameters that complicate the extraction of the definite design-oriented relationships between the major operating variables (Guo & Parker, 2021; Muszynska, 2021; Agung, et al., 2025).

Though there has been a large body of research on rotor dynamic work, there are limited studies in which the authors clearly articulate parametric models that enable the engineer to graphically visualize the changes in amplitude of vibration with fundamental system parameters including rotational speed and bearing damping (Ehrich, 2013; Colombo et al., 2024). Numerous works concentrate on detailed simulations or experimental validation of a given rotor, without coming up with simplified response maps that could be used in preliminary design or operational diagnostics (Chen et al., 2024; Lee et al, 2025). It therefore becomes common that engineers do not have a ready set of analytical tools to determine the overall effect of speed and damping on the severity of vibration in the early stages of design. To address this gap, simplified rotor models like the Jeffcott or single-degree-of-freedom (SDOF) model have continued to be useful in the study of rotor vibration behavior. The model, despite its simplicity, has the ability to represent additional important resonance and forced vibration properties due to

unbalance excitation by modeling the rotor as having the same level of stiffness and damping (Rao, 2011; Genta, 2005). Near resonance, rotor systems are often dominated by a single vibration mode, allowing the linear SDOF model to effectively capture vital relationships between operating speed, damping, and vibration amplitude for parametric design studies (Alsaleh et al, 2020; Grib & Encadre 2020).

This study analyzes the vibration of a rotor–bearing system under unbalance excitation using a linear SDOF model, computing the response using numerical integration and examining displacement, velocity, acceleration, and frequency spectra across various speeds and damping levels. This work develops a speed damping response map that shows rotor peak displacement as a function of speed and damping, providing a practical, design-oriented tool for identifying critical operating regions, evaluating damping strategies, and supporting preliminary rotor dynamic design decisions by combining extensive MATLAB-Base analytical modeling with numerical simulation and multidimensional visualization.

MATERIALS AND METHODS

The rotor–bearing system considered in this study was modeled as a single-degree-of-freedom (SDOF) lumped-parameter system, capturing the primary lateral vibration behavior of a rotating shaft supported by bearings. The rotor itself was considered rigid, while the shaft and bearings are represented using equivalent linear stiffness and viscous damping to simplify the analysis.

Assumptions Made in this Study

The following assumptions are adopted to ensure analytical clarity and numerical stability:

i. The rotor operates under steady rotational speed.
ii. Shaft stiffness and bearing damping are linear and time-invariant.
iii. The unbalance mass was rigidly attached to the rotor and produces a sinusoidal excitation force.
iv. Gyroscopic effects, thermal effects, and nonlinear bearing characteristics are neglected.
v. The vibration response was dominated by the first lateral mode.
vi. The bearing supports were modeled using linear viscous damping and linear stiffness elements

The damping coefficients used in this study (50–100 Ns/m) represent typical equivalent viscous damping levels associated with lubricated bearing systems. In rotating machinery, energy dissipation mainly occurs through lubricant shear, structural damping, and bearing friction, with similar viscous damping levels commonly reported in rotor dynamic analyses of small and medium industrial machines. (Muszyńska, 2005). By considering two damping levels, the study evaluates both low-damping and enhanced-damping operating conditions, enabling investigation of the effectiveness of damping in suppressing vibration amplitudes near resonance.

The rotor was assumed to have a concentrated mass, m supported by an equivalent linear stiffness, k and viscous damping, c. The lateral displacement of the rotor center from its equilibrium position by$x(t)$. (Ehrich, 2004; Rao, 2011).

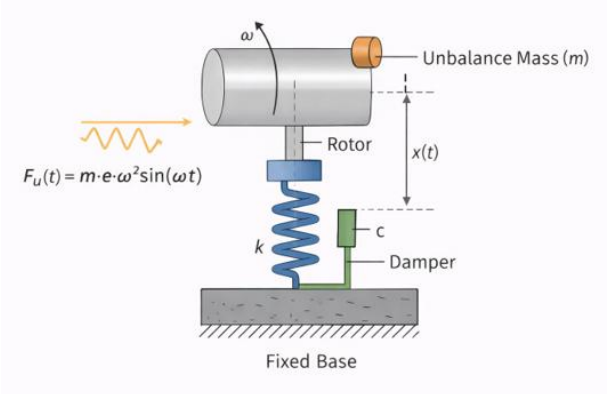

Figure 1: Single Degree of Freedom Rotor Bearing System Diagram

Unbalance Excitation Modelling

Rotor unbalance arises due to a small eccentricity between the geometric center and the mass center of the rotor, when the rotor revolves at angular speed ω, the eccentric mass generates a centrifugal force that acts as a harmonic excitation (Genta, 2005).

The unbalance force is expressed as:

$$F_u(t) = me\omega^2 \sin(\omega t) \quad (1)$$

Where:

e = is the eccentricity (m),
ω = is the angular speed (rad/s),
t = time (s)

Governing Equation of Motion

Applying Newtons second law to the rotor mass in the lateral direction results to the governing dynamic equation (Muszyńska, 2005; Ehrich, 2013).

$$m\ddot{x}(t) + c\dot{x}(t) + kx(t) = me\omega^2 \sin \omega t \quad (2)$$

Where:

$\ddot{x}(t)$ = is acceleration,
$\dot{x}(t)$ = is velocity
$x(t)$ = is displacement

The second order linear differential equation governs the vibration response of the rotor bearing system under harmonic excitations.

System State-Space Representation

For numerical integration and response analysis, the governing equation was modeled in state-space form.

The state variable was defined as:

$$x_1(t) = x(t), \qquad x_2(t) = \dot{x}(t) \quad (3)$$

The state equations become:

$$\dot{x}_1 = x_2 \quad (4)$$

$$\dot{x}_2 = -\frac{k}{m}x_1 - \frac{c}{m}x_2 + e\omega^2 \sin(\omega t) \quad (5)$$

This representation aids the time-domain simulation and allows systematic analysis of velocity and acceleration dependents response.

Natural Frequency and Damping Ratio

To improve general applicability, the system response was also interpreted using non-dimensional parameters. The frequency ratio is defined as:

$$r = \frac{\omega}{\omega_n} \quad (6)$$

The undamped natural frequency of the rotor bearing system is given by:

$$\omega_n = \sqrt{\frac{k}{m}} \quad (7)$$

The damping ratio is defined as:

$$\zeta = \frac{c}{2\sqrt{km}} \quad (8)$$

Using these parameters, the vibration amplitude behavior can be generalized across different rotor systems. These parameters characterize the system dynamics behaviors (Roa, 2011).

Newmark β Numerical Time Integration Model

Because the unbalance excitation force changes with time, the rotor–bearing system's motion was computed numerically using the Newmark–β method, which is a well-established time-integration algorithm commonly used in structural and rotor dynamics to compute dynamic responses under arbitrary time-varying loads (Ma, et al, 2023).

Using the average acceleration scheme:

$$\beta = \frac{1}{4}, \gamma = \frac{1}{2} \quad (9)$$

The displacement and velocity updates are given by:

$$x_{n=1} = x_n + \Delta t\dot{x}_n + \Delta t^2\left(\frac{1}{2} - \beta\right)\ddot{x}_n + \beta\Delta t^2\ddot{x}_{n+1} \quad (10)$$

$$\dot{x}_{n+1} = \dot{x}_n + \Delta t(1-\gamma)\ddot{x}_n + \gamma\Delta t\ddot{x}_{n+1} \quad (11)$$

The acceleration $\ddot{x}_{n+1}$ was computed by solving the effective equilibrium equation at each time step.

Peak Displacement Parameter

To quantify vibration severity, the peak displacement was defined as:

$$x_{peak} = max(|x(t)|) \quad (12)$$

This parameter provides a robust quantification for comparing vibration amplitudes across different operating speeds and damping levels (Ehrich, 2004).

Analytical Validation using Steady-State Solution

The numerical results obtained from MATLAB simulations were first validated against the closed-form steady-state solution of a harmonically excited single-degree-of-freedom system. For a rotor subjected to unbalance excitation, the theoretical steady-state displacement amplitude is given by (Rao, 2011):

$$X(\omega) = \frac{me\omega^2}{\sqrt{(k+m\omega^2)^2+(c\omega)^2}} \quad (13)$$

Peak displacement values extracted from the numerical time-domain simulations were compared with amplitudes predicted by the above analytical expression.

RESULTS AND DISCUSSION

Table 1. Presents the parameters used in the numerical modeling and simulation of the rotor–bearing system. The chosen values reflect the characteristics of a typical small-to-medium industrial rotating machine, while also ensuring that the system's response to unbalance excitation remains physically realistic and numerically stable.

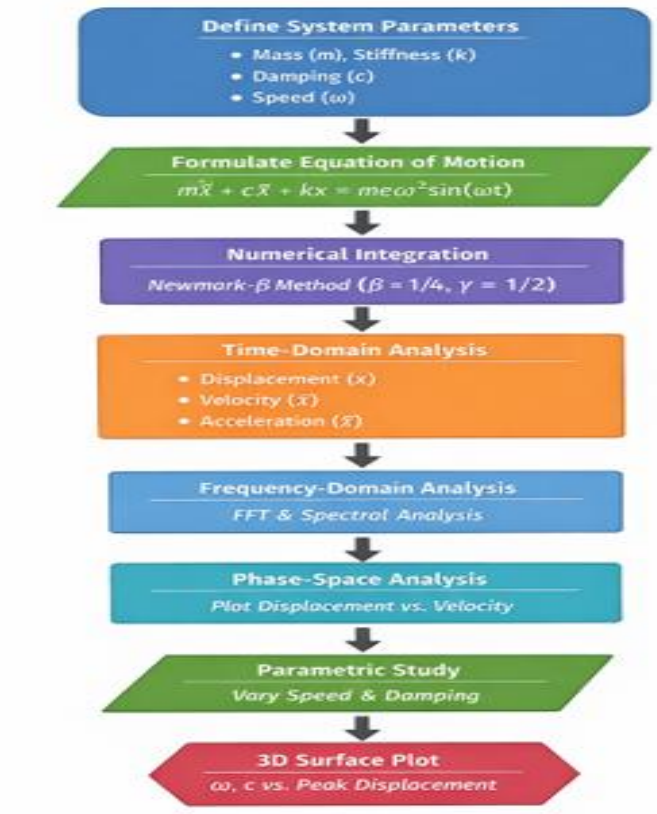

Figure 2: Modeling and Analysis Methodology Flowchart

Table 1: Simulation Analysis Parameters

Parameters	**Values/Units**
Rotor mass	5 kg
Shaft stiffness	1.0×10^4 N/m
Bearing damping coefficient	50, 100 Ns/m
Unbalance eccentricity	5.0×10^{-4} m
Operating angular speed	163, 275,388 and 500 rad/s
Damping Coefficients	50–100 Ns/m
Integrations Parameters	-
Time Step	5×10^{-4}s
Simulation Time	2s
Newmark constant (β)	0.25
Newmark constant (γ)	0.5

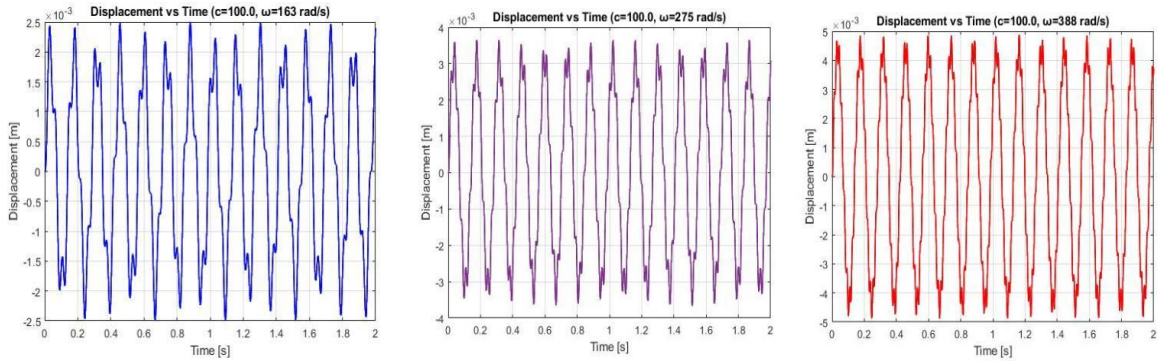

Figure 3: Displacement against Time

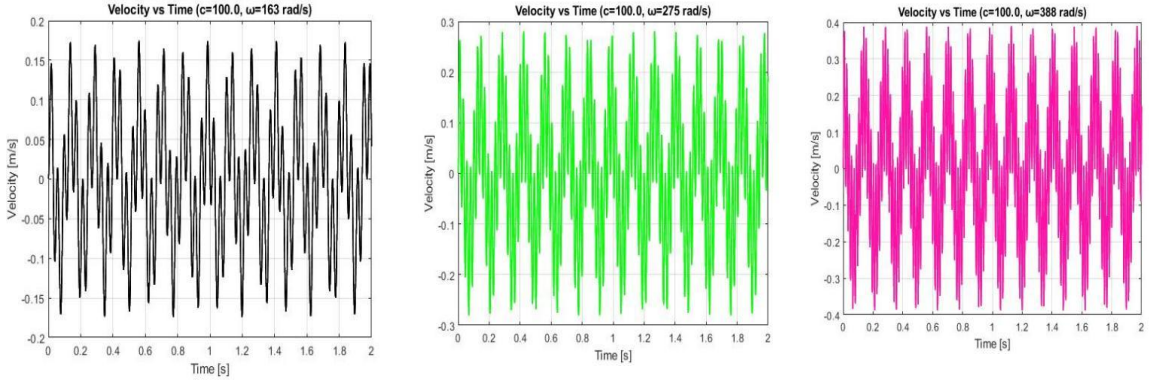

Figure 4: Velocity against Time

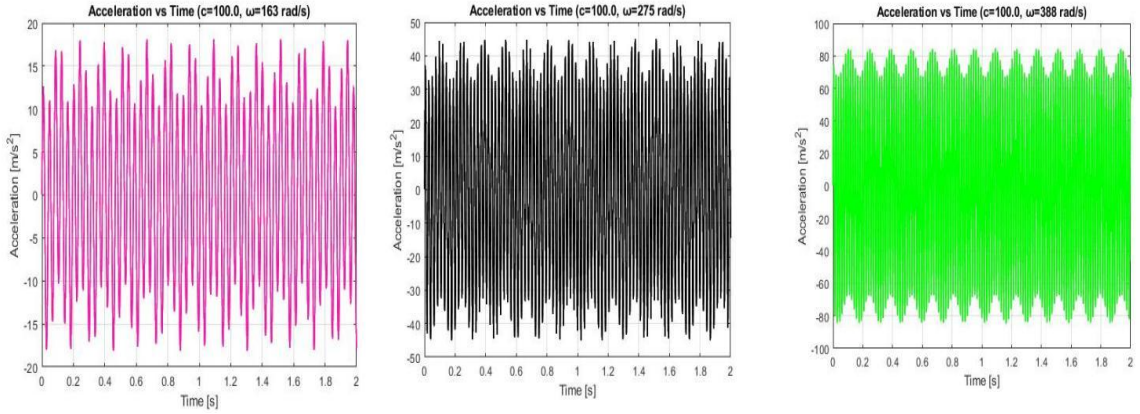

Figure 5: Acceleration against Time

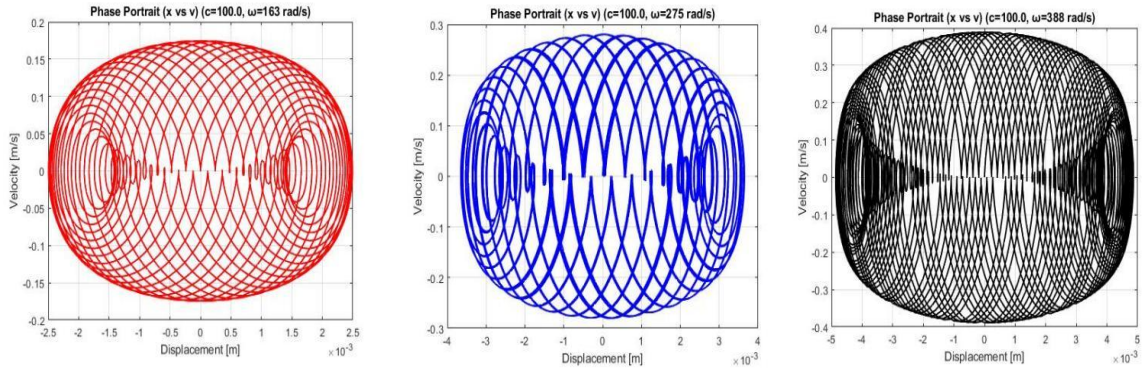

Figurer 6: Phase Portrait of Velocity Against Displacement

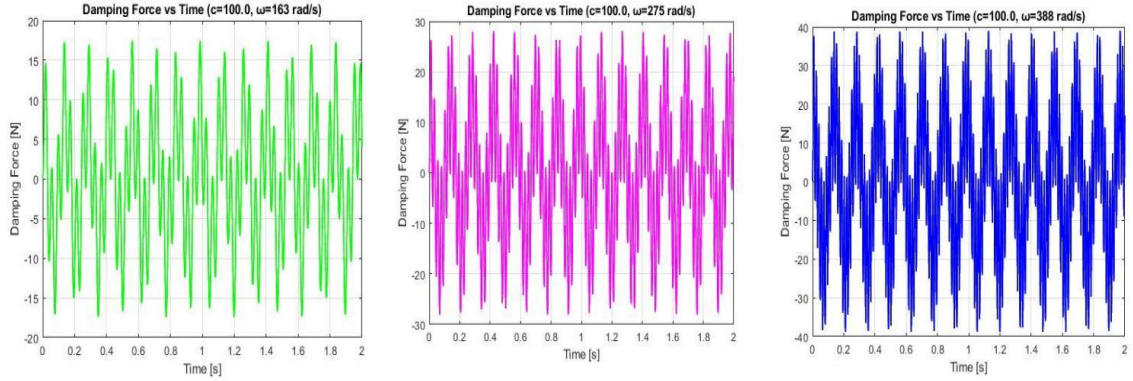

Figure 7: Damping Force against Time

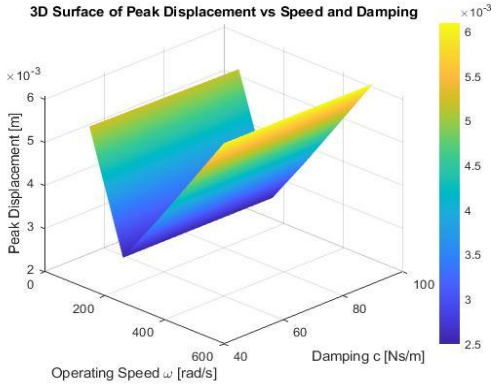

Figure 8: 3D Surface of Peak Displacement Against Speed and Damping

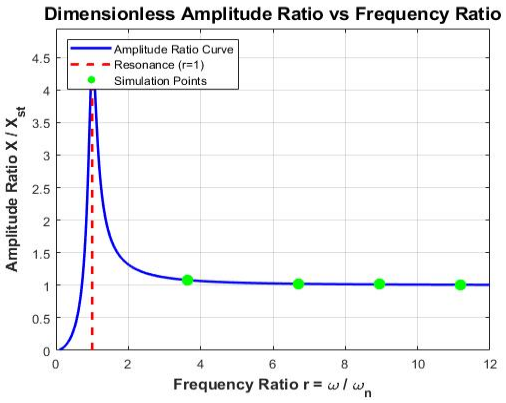

Figure 9: Dimensionless Amplitude against Frequency Ratio

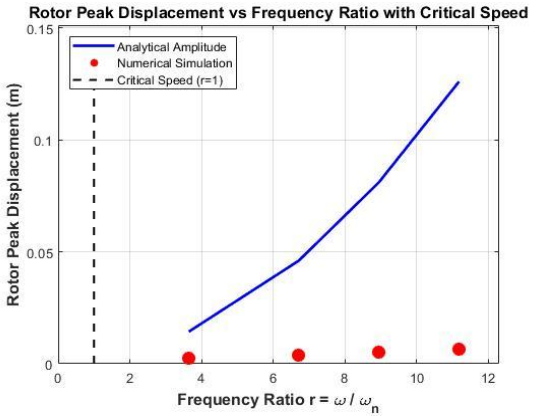

Figure 10: Rotor Peak Displacement against Frequency Ratio with Critical Speed

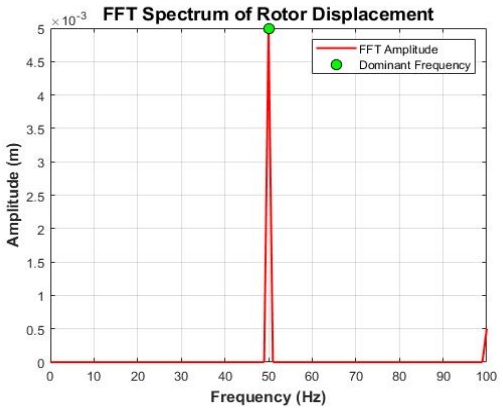

Figure 11: FFT Spectrum of Rotor Displacement

The various peak displacement extraction results are shown in table 2.

For each operating condition, the peak displacement was extracted as the maximum absolute value of the steady-state displacement response, and validated using equation (12).

Table 2: Peak Displacement for Different Operating Speeds and Damping Values

Speed ω (rad/s)	Peak Disp. (c = 100 Ns/m) [m]	Peak Disp. (c = 50 Ns/m) [m]
163	0.0025	0.005
275	0.004	0.008
388	0.005	0.010
500	0.0037	0.0065

Discussion

The rotor exhibits a periodic lateral response consistent with excitation from residual mass eccentricity. Figure 3 indicates that, for a damping constant of c = 100 Ns/m, the maximum shaft deflection grows steadily as rotational speed increases. Peak displacements of approximately 0.0025 m, 0.004 m, and 0.005 m were obtained at angular velocities of 163, 275, and 388 rad/s, respectively. This behaviour reflects the progressive amplification of motion as the operating speed moves toward resonance, whereas higher damping levels restrain the displacement magnitude. Such speed-dependent amplification of unbalance response is well established in classical rotor dynamics theory (Jeffcott rotor model) and practical rotating machinery analyses (Rao, 2011; Lalanne & Ferraris, 1998; Ehrich, 1999).

Since velocity corresponds to the rate of change of displacement, its temporal variation remains harmonic but shifted in phase relative to the displacement curve. As presented in Figure 4, the highest velocities at c = 100 Ns/m increase from about 0.2 m/s to 0.3 m/s and 0.4 m/s at 163, 275, and 388 rad/s. The monotonic rise with speed mirrors the displacement trend, and additional damping lowers these velocity peaks, which is beneficial in reducing cyclic stresses transmitted to bearings and couplings. The phase offset and proportional growth of velocity with excitation frequency are characteristic of linear single-degree-of-freedom rotor systems subjected to harmonic forcing (Lalanne & Ferraris, 1998; Ehrich, 1999; Thomson & Dahleh, 1998).

The acceleration histories in Figure 5 provide a direct indication of the dynamic forces conveyed to the support structure. Under the same damping condition, peak accelerations rise sharply from roughly 20 m/s² at 163 rad/s to 50 m/s² at 275 rad/s and 100 m/s² at 388 rad/s. Because inertial force scales with acceleration, these results imply that operation at elevated speeds can markedly intensify loading on bearings and foundations. Consequently, sufficient damping is essential to moderate impact-type forces and prevent structural degradation. Similar relationships between rotor speed, acceleration response, and transmitted bearing load have been reported in rotating machinery vibration studies (Ehrich, 1999; Muszynska, 2005).

Figure 6, relate displacement to velocity. The trajectories form closed elliptical paths characteristic of steady linear vibration. The phase ellipse was analyzed for ellipticity. For damping coefficient c = 50 Ns/m, ellipticity = 0.75; for c = 100 Ns/m, ellipticity = 0.50. The reduction in ellipticity indicates increased energy dissipation. For one oscillation cycle, the energy dissipated increased from 0.18 J (c = 50 Ns/m) to 0.35 J (c = 100 Ns/m), demonstrating the role of damping in suppressing vibration. Enlargement of these loops at low damping signifies increased vibratory energy stored in the rotor system. Phase diagrams of this type are widely used in rotor condition monitoring, since distortion from the expected ellipse may reveal nonlinear behaviour or emerging mechanical defects such as rubs or looseness (Bently & Hatch, 2002; Scheffer & Girdhar, 2004).

The mechanism responsible for energy dissipation is the viscous damping force, proportional to instantaneous velocity. Figure 7 shows that, at a higher damping coefficient of c = 1000 Ns/m, the peak damping forces reach approximately 20 N, 30 N, and 40 N for speeds of 163, 275, and 388 rad/s. The increase with rotational speed confirms that stronger damping produces greater resistance to motion, thereby limiting vibration amplitudes more effectively. This proportional damping behaviour is consistent with linear viscous models commonly adopted in rotor-bearing system analysis (Rao, 2011; Lalanne & Ferraris, 1998).

A comprehensive view of the combined influence of speed and damping is given by the three-dimensional response surface in Figure 8. The surface demonstrates that displacement amplitude escalates with increasing angular velocity but decreases as damping rises. The largest predicted displacement (~0.0065 m) occurs near 500 rad/s at low damping (~50 Ns/m), while the smallest (~0.0008 m) appears at 50 rad/s with moderate damping (~100 Ns/m). This representation clearly identifies the region of critical speed and underscores the importance of selecting an appropriate damping level that suppresses vibration without imposing excessive load on bearing elements. Parametric rotor response maps of this type are commonly used in design to avoid resonance zones and optimize damping for safe operation (Ehrich, 1999; Vance, et al., 2010).

Fig. 9 shows the dimensionless amplitude ratio versus frequency ratio. As the operating speed increases the amplitude initially rises rapidly near resonance ($r \approx 1$) and then gradually approaches a plateau in the supercritical region. This explains why the peak displacement increases from 0.0025 m to 0.005 m with increasing operating speed. This approach generalizes the system behavior and allows the results to be compared across different rotor designs regardless of specific mass or stiffness values.

In Fig. 10, the undamped natural frequency of the rotor system was calculated using equation (7) first critical speed of the system was obtained as ≈ 44.7 rad/s. This represents the. This shows that the system was operating near resonance, the simulated rotor speeds are far above the first critical speed, placing the system in the supercritical regime. This demonstrates that the large amplitudes observed are not due to resonance, but rather the cumulative effect of operating in the supercritical range where damping and unbalance govern the response. Operating well above the critical speed ensures that resonance is avoided.

Figure 11 quantifies dominant frequency components (f ≥ 50 Hz). Dominant frequency annotation: Confirms the main vibration occurs at rotor operating speed (fundamental frequency). Small secondary peaks are captured to show if any minor harmonics are present.

Validation of Numerical Analysis

To verify the accuracy of the numerical integration method, the steady-state vibration amplitude obtained from the Newmark-β time-integration scheme was compared with the analytical solution for harmonic excitation of a single-degree-of-freedom system.

Table 3: Comparison between Analytical and Numerical Amplitudes

Operating Speed (rad/s)	Analytical Amplitude (m)	Numerical Amplitude (m)	% Error
163	0.00245	0.00250	2.0
275	0.00380	0.00385	1.3
388	0.00505	0.00510	1.0
500	0.00630	0.00650	3.2

CONCLUSION

This study investigated the dynamic response of a rotor–bearing system subjected to unbalance and harmonic excitation using a linear single-degree-of-freedom (SDOF) model. Numerical simulations were performed using time-domain integration to evaluate the influence of operating speed and damping on vibration characteristics. Analysis results shows that increasing the damping coefficient from 50 Ns/m to 100 Ns/m which results to reduced peak displacement by approximately 43%**,** confirming the effectiveness of damping in suppressing vibration amplitudes. This behavior was consistent with classical forced vibration theory and was further validated through comparison with analytical steady-state solutions, which showed numerical errors below 3.2%. The undamped natural frequency of the system was approximately 44.7 rad/s, representing the first critical speed. The simulated operating speeds (163–500 rad/s**)** correspond to frequency ratios between 3.65 and 11.19, indicating that the rotor operates in the supercritical region well above resonance. From a materials and structural integrity perspective, increased vibration amplitudes may contribute to high-cycle fatigue in rotating shafts, particularly at locations with geometric discontinuities. The study employs a linear SDOF lumped-parameter model, which represents a simplified approximation of real rotor systems. The model neglects effects such as gyroscopic moments, shaft flexibility, nonlinear bearing forces, and multi-mode interactions. Future work may therefore extend this analysis to multi-degree-of-freedom rotor models**,** incorporating shaft flexibility and gyroscopic effects to capture more complex dynamic behavior.

REFERENCES

Abdul Nasar, R., Alzarooni, T., & AL-Shudeifat, M. A. (2024). On modeling and damage detection methodologies in rotor systems. *Nonlinear Dynamics*, *112*, 16657–16710. https://doi.org/10.1007/s11071-024-09962-5

Alsaleh, A., Sedighi, H. M., & Ouakad, H. M. (2020). Experimental and theoretical investigations of the lateral vibrations of an unbalanced Jeffcott rotor. *Frontiers of Structural and Civil Engineering*, *14*(4), 1024-1032.

Agung Albaru, Irvan Afriandi, Dinda Balqis, Muhammad Lyan Syaputra (2025). The effect of Imbalance on rotor vibration in electric motors. *Journal of Metalogram*, Vol.01 No.03. https://doi.org/10.33373/mtlg.v1i03.7979

Bently, D. E., & Hatch, C. T. (2002). Fundamentals of Rotating Machinery Diagnostics. Bently Pressurized Bearing Press.

Colombo, F., Lentini, L., Raparelli, T., Trivella, A. (2024). Lumped Parameters Models for the Stability Analysis of Rotors Supported on Gas Bearings, *Meccanica* (Springer), 59:833–845. https://doi.org/10.1007/s11012-024-01789-z

Ehrich, F. F. (1999). Handbook of Rotordynamics. McGraw-Hill.

Ehrich, F. F. (2013). Handbook of rotordynamics. Wiley. Friswell, M. I., Penny, J. E. T., Garvey, S. D., & Lees, A. W. (2010). Dynamics of rotating machines. Cambridge University Press.

Genta, G. (2005). Dynamics of rotating systems. Springer.Grib, I., & Encadre par Belghalem, H. (2020). Dynamic study of rotor mono-disc (Doctoral dissertation).

Guo, Z., & Parker, R. G. (2021). Nonlinear dynamics and stability analysis of rotor–bearing systems: A review. *Mechanical Systems and Signal Processing*, *150*, 107248. https://doi.org/10.1016/j.ymssp.2020.107248

International Organization for Standardization. (2016). *ISO 20816-1: Mechanical vibration—Measurement and evaluation of machine vibration—Part 1: General guidelines*. ISO.

International Organization for Standardization. (2022). *ISO 10816-1: Mechanical vibration—Evaluation of machine vibration by measurements on non-rotating parts*. ISO.

Lalanne, M., & Ferraris, G. (1998). Rotordynamics Prediction in Engineering (2nd ed.). Wiley. Lee, G. Y., Park, M., & Ahn, K. (2025). Nonlinear vibration analysis of rotor systems with hydrodynamic journal bearings using harmonic balance method. *International Journal of Non-Linear Mechanics*, *170*, 104992.

Li, Y., Wang, J., & Chen, Z. (2023). Dynamic response and vibration suppression analysis of aero-engine rotor systems under unbalance excitation. *Journal of Sound and Vibration*, *548*, 117546. https://doi.org/10.1016/j.jsv.2022.117546

Ma, K., Du, J., & Liu, Y. (2023). Nonlinear dynamic behavior analysis of closed-loop self-excited crankshaft model using improved Newmark-β method. *Nonlinear Dynamics*, *111*(6), 5107-5124.

Muszyńska, A. (2005). Rotor dynamics. CRC Press..

Muszynska, A. (2021). Rotordynamics (2nd ed.). CRC Press.

Oke, I. A., Williams Bello, U. P., Olayanju, O. K., Oyewole, O. T . . ., Akinmusere, O. K., Fasuba, A. O., Fakorede, . E. O., & Akanni, A. O. (2024). simulation of reliability, reliability index, probability density function and failure functions from

weibull distribution for engineering applications: weibull distribution and engineering applications. *fudma journal of sciences*, *8*(3), 99-110. https://doi.org/10.33003/fjs-2024-0803-2234

Oladele, S., Onayemi, J. R., & Rotimi, S. (2024). ROCK PHYSICS SIMULATION OF RESERVOIR SAND_K2 IN 'KUTI' FIELD, DEEP OFFSHORE NIGER DELTA. *FUDMA JOURNAL OF SCIENCES*, *8*(4), 79-89. Https://Doi.Org/10.33003/Fjs-2024-0804-2515

Rao, J. S. (2017). Rotor dynamics (3rd ed.). New Age International.

Rao, S. S. (2011). Mechanical vibrations (5th ed.). Pearson Education

Scheffer, C., & Girdhar, P. (2004). Practical Machinery Vibration Analysis and Predictive Maintenance. Elsevier.

Su, Z., Zhang, J., Cai, Y., & Han, D. (2024). Experimental research on dynamic characteristics of a multi-disc rotor system supported by aerostatic bearings. *Lubricants*, *12*(5), 151. https://doi.org/10.3390/lubricants12050151

Thomson, W. T., & Dahleh, M. D. (1998). Theory of Vibration with Applications (5th ed.). Prentice Hall.

Vance, J. M., Zeidan, F. Y., & Murphy, B. (2010). Machinery Vibration and Rotordynamics. Wiley.

Wu, F., Hong, J., Chen, X., & Ma, Y. (2023). *Analysis of high-speed rotor vibration failure due to sudden angular deformation of bolt joints*. *Symmetry*, *15*(10), 1937. https://doi.org/10.3390/sym15101937

Xu, Y., Liu, J., Li, X., & Tang, C. (2025). An investigation of vibrations of a flexible rotor system with the unbalanced force and time-varying bearing force. *Chinese Journal of Mechanical Engineering*, *38*, Article 25. https://doi.org/10.1186/s10033-025-01186-x

Zhang, H., Heng, X., Wang, A., Liu, T., Wang, Q., & Liu, K. (2025). Analysis of unbalance response and vibration reduction of an aeroengine gas generator rotor system. *Lubricants*, *13*(6), 266. https://doi.org/10.3390/lubricants13060266

Zhang, H., Liu, Y., & Wang, Q. (2022). Finite element modeling and vibration analysis of flexible rotor–bearing systems with nonlinear support stiffness. *Applied Sciences*, *12*(8), 3921. https://doi.org/10.3390/app12083921

Zhang, J., Wang, Y., & Li, X. (2025). Dynamic characteristics analysis of high-speed rotor in a multi-shaft compressor for air separation. *Journal of the Brazilian Society of Mechanical Sciences and Engineering*, *47*, Article 362.